

**Yearly Progress Report (August 2019):
Plasma Surface Interactions: Predicting the Performance and Impact of Dynamic PFC Surfaces**

Lead PI: Brian Wirth, UTK-ORNL Governor's Chair Professor of Computational Nuclear Engineering

<i>Institution – Agreement/FWP #</i>	<i>Principal Investigator</i>	<i>Senior Personnel</i>
ORNL - ERAT953	Brian Wirth	David Bernholdt, John Canik, Philip Fackler, David Green, James Kress, David Pugmire, Pablo Seleson, Clayton Webster
ANL –	Barry Smith	Shashi Aithal
LLNL - SCW1617 / SCW1620	Ilon Joseph	Mikhail Dorf, Milo Dorr, Maxim Umansky
LANL -	Enrique Martinez	Sham Bhat, Danny Perez, Arthur Voter
PNNL – FWPs 70444/70230	Wahyu Setyawan	Giridhar Nandipati, Ken Roche
SNL – FWPs 18-020352/18-020349	Habib Najm	Tiernan Casey, Mary Alice Cusentino, Khachik Sargsyan, Aidan Thompson, Mitch Wood
GA – DE-SC0018423	Phil Snyder	Rui Ding, Jerome Guterl, Orso Meneghini
UCSD – DE-SC0018302	Sergei Krasheninnikov	Russ Doerner, Roman Smirnov
UIUC – DE-SC0018141	Davide Curreli	Jon Drobny, Rinat Khaziev
UMass Amherst – DE-SC0018421	Dimitrios Maroudas	Chao-Shou Chen, Asanka Weerasinghe
UMissouri	Karl Hammond	Brandon Laufer
University of Tennessee, Knoxville	Brian Wirth	Sophie Blondel, Dwaipayan Dasgupta, Ane Lasa, David Martin, Li Yang, Tim Younkin
RPI -	Mark Shephard	Onkar Sahni, Gopan Perumpilly

Executive Summary

This document describes the integrated project progress during the second year of the project, focusing on the time period from the first year report submitted in May 2018 until the end of June 2019. Overall, the PSI SciDAC project had a very productive and impactful year, with highlights including:

- Successful completion of the FY2018 Fusion Theory and Simulation Milestone on Plasma Materials Interaction to meet the DOE FES Fusion Theory Performance Measure Management milestone [1];
- Organization of a well attended mini-conference on Plasma Surface Interactions at the 2018 APS-DPP meeting in Portland, OR in November 2018 [2];
- Strong engagement with the ITER Divertor and Plasma-Wall Interactions Section, led by Richard Pitts;
- Visit to the WEST tokamak and ITER in January 2019, which established a new collaboration with CEA for experimental validation of PSI SciDAC models on the all metal WEST tokamak, and continued collaborative interactions with the ITER Divertor and Plasma-Wall Interactions Section;
- Annual team project meeting to review status and prioritize next steps held jointly with the AToM project in February 2019 at General Atomics;
- Multiple oral presentations and strong project presence at the 2019 Plasma Facing Components Conference in Eindhoven, Netherlands in May;

- Publication of 17 peer-reviewed, archival journal publications, as listed in Appendix 1; one of which was an Editor's pick (Krasheninnikov, *Physics of Plasmas* **25** (2018) 064501), another one was a Feature Article (Yang and Wirth, *Journal of Applied Physics* **123** (2018) 215104), and a third one was an invited review paper (Maroudas and Wirth, *Current Opinion in Chemical Engineering* **23** (2019) 77-84).

The remainder of this document presents a brief review of the project objectives, and then provides a concise summary of the research activities as organized by research task (Note that in the interest of brevity, this summary is not comprehensive, but rather conveys highlights of research activities to provide an indication of the breadth of the project activities), and then concludes with the next steps planned for each task.

Introduction and Background

The objective of this project is to develop, and integrate, high-performance simulation tools capable of predicting plasma facing component (PFC) operating lifetime and the impact of the evolving surface morphology of tungsten-based PFCs on plasma contamination, including the dynamic recycling of fuel species and tritium retention, in future magnetic fusion devices. Establishing a fundamental physical understanding and developing predictive capabilities of plasma-surface interactions (PSI) requires simultaneously addressing complex and diverse physics occurring over a wide range of length (Angstroms to meters) and time (femtoseconds to years) scales, as well as integrating extensive physical processes across the plasma – surface interface. This requires development of not only detailed physics models and computational strategies at each scale, but also algorithms and methods to couple them effectively in a way that can be robustly validated. Deploying these tools requires the continued development and coupling of leadership-scale computational codes to describe the boundary plasma and the evolving PFC surface, as well as a host of simulations that bridge disparate scales to address complex physical and computational issues at the plasma – surface interface in multi-component materials systems for magnetic fusion energy development beyond ITER.

This project will enable discovery of the key physical phenomena controlling critical PFC performance issues, and the quantitative prediction of their impact on PFC performance during both steady-state and transient plasma conditions. Such phenomena include: (i) surface evolution in regions of either net erosion or net deposition; (ii) the impact of the evolving surface composition and roughness on the retention and recycling of hydrogenic fuel isotopes; (iii) the impact of dilute impurities on surface morphological evolution and plasma contamination; and (iv) the effects of high-energy neutron damage on surface properties that could influence helium/hydrogenic species retention and recycling. The research activities within this proposed project will focus on three broadly defined research thrusts:

- Bridging the scales between atomistic/microstructural modeling and the continuum-based PFC simulations through the adaptation of multiscale modeling techniques. Specifically, *ab initio*/atomistic/microstructural studies will be used to develop the requisite knowledge to ‘coarse grain’ disparate, heterogeneous material structures and ‘scale bridge’ across diverse spatial/temporal scales to provide detailed input to, and calibrate, the Xolotl PFC simulator;
- Integrating boundary plasma and surface evolution models, specifically investigating effects of the plasma sheath and evolving surfaces, in order to predict PFC performance under both steady-state plasma operation and in the presence of transient events. This includes the development of a new code to model the fate of eroded impurities, including their migration and re-deposition, specifically designed to take advantage of leadership-class computing facilities; and
- Studying the dynamic response of the surface to transient plasma events and exploring synergistic phenomena between the near-surface plasma and wall response, with emphasis on dynamic recycling processes that couple the divertor plasma to the material surface layer. The coupled models will explore the impact of wall response on boundary turbulence and divertor detachment dynamics.

The outcome of this project will be a suite of coupled plasma and materials modeling tools, and a leadership class PFC simulator to predict PFC evolution and feedback to the boundary plasma both during steady-state plasma operation and transient events. Towards this end, we plan to have strong coordination of our efforts with the other successful fusion SciDAC projects proposals in the Boundary Physics and Whole Device Modeling topical areas. Success in the proposed research tasks will enable the prediction of both plasma fueling and the sources of impurity contamination that impact core plasma performance, and will lay the foundation for understanding, designing and developing the materials required to meet the performance objectives of future fusion reactors.

The project has established a web presence at: <https://collab.cels.anl.gov/display/PSIscidac2/> leveraging R&D infrastructure available in the ANL Mathematics and Computer Sciences Division. This wiki site has both public-facing and project-private spaces. Currently, the public space provides basic information about project goals, participants, sponsors, key collaborators, and a catalog of project presentations and publications. The private space includes records of project and working group meetings and other information. Additionally, we use a Subversion repository, also hosted at ANL, as a repository for internal and under-development documents, and the project mailing list hosted at ORNL.

This document describes the integrated project progress during the time period from the second year from the first year report submitted in May 2018 until the end of June 2019, and includes discussion on the status of specific tasks on both the applied mathematics/computer science and domain physics aspects of the program, and then concludes with the next steps planned for each task.

STATUS AND INITIAL PROGRESS ON PROJECT RESEARCH ACTIVITIES

Computer Science/Applied Math

Computer science and applied math (CS/AM) are strongly driven by the science goals of the project and are well integrated through the three major Tasks described below. In this section, we call out and describe certain of these activities in greater detail in order to illustrate the engagement and interactions within the project. We would also like to note our engagement with researchers at Rensselaer Polytechnic Institute (RPI) as part of Task 2, where the current focus is on infrastructure development in support of parallel, unstructured meshing for particle in cell (PIC) calculations. They are providing a separate progress report, which encompasses their work on multiple SciDAC projects.

Computational readiness for large-scale MD and KMC simulations: This work, carried out by Ken Roche (PNNL), focuses on improving the computational performance and GPU implementation of the codes used within the SciDAC project, and has also involved activities at Sandia National Laboratories (led by Aidan Thompson) to optimize the performance of machine-learning SNAP interatomic potentials in the LAMMPS code. These activities effectively support MD analysis of helium – hydrogen interactions in mixed tungsten – beryllium surfaces in Task 1.

We have executed and reproduced the correct output for a 2000 W atom test system using a custom-built LAMMPS and stand-alone sequential SNAP (2J8) potential on Intel KNL nodes. The execution of the stand-alone SNAP potential has been profiled to identify inefficiencies and potential optimizations. The findings have been discussed with a team from NERSC who have aptly optimized this test implementation with OMP threads. Testing and profiling the Kokkos-based GPU accelerated SNAP implementation is ongoing and should be completed on the Summit machine this FY.

In another effort, we are pursuing how to speed-up and increase the volume modeled within the Object Kinetic Monte Carlo (OKMC) method for defect evolution modeling as implemented in the KSOME software. A domain decomposed OKMC variant using Pthreads designed for shared memory multicore

hardware targets is being prototyped for testing. In this approach, each sub-domain can evolve independently, but the challenges include the regular computation of global simulation time and synchronization at sub-domain boundaries which can lead to backtracking the evolution (a step that imposes limitations on parallel speedups for this algorithm). For performance reasons, we want to compare the approaches taken for reaction event computation table updates on multicore hardware and a CUDA implementation designed for GPU accelerated nodes.

Development of unstructured meshing capability for hPIC and GITR: The RPI team is developing mesh related capabilities required for two classes of PIC calculations: i) impurity transport, and ii) plasma sheath/pre-sheath. For impurity transport calculations a new mesh-based PIC approach is being employed while for sheath/pre-sheath region a new multi-block boundary layer mesh capability is being developed.

As part of the SciDAC 4 fusion projects, the RPI team is developing an unstructured mesh-based approach for PIC calculations that is being used in the development of a version of the impurity transport code GITR, based on the mesh-based PIC approach. The new code is referred to as the GITRm code. The overall plan is to progressively incorporate the full set of physics capabilities and numerical algorithms being used in the current GITR code and to then support additional physics capabilities and couplings as desired by the PSI2 team.

The structures and geometric operations of the mesh-based PIC approach are encapsulated under the PUMIpic library. Our focus thus far in the development of GITRm has been on getting an operational workflow that includes all key operational steps building on using PUMIpic. However, on the first pass, the physics for specific steps is simplified. The plan is to progressively reach a fully featured workflow by implementing each operation in full detail.

At the core of the new mesh-based PIC approach resides a set of mesh and particle representations and algorithms to perform the necessary geometry centric operations associated with the interactions of the particles with the mesh, and the mesh with the particles, in a fully parallel fashion. The design goals for PUMIpic are:

1. Support a method in which both the mesh and particles can be distributed. However, to define the mesh distribution such that interprocess communication is avoided during the core operations of a single PUSH step. This is done by having sizable overlaps of neighboring portions of the mesh.
2. Employ data structures relating the particles and mesh that are effective on accelerator based systems.
3. Take advantage of geometry-based algorithms that are effective for general (graded) unstructured meshes over geometrically complex domains.

To satisfy the first design goal, the core representations of the mesh and particles cannot be independent as is common in most PIC codes where the relationships between them is through a background grid. (In addition, a uniform background grid is not effective when graded meshes are used.) In PUMIpic the mesh is the core structure and access to the particles is through the mesh entities they currently reside within. PUMIpic is being designed to support distributed meshes where each PICpart is defined as a core part and a set of surrounding parts to have sufficient buffer to avoid needing communicate during a PUSH step.

Our developments so far on GITRm have been focused on the following six key operations: field-following mesh generation, particle initialization, field evaluation and interpolation, near-boundary fields, particle push using Boris move and particle-boundary interactions. At this time particle initiation is somewhat arbitrary, field interpolation is based on a linear basis in 3D Cartesian coordinates and the particle-boundary intersection is based on the straight-sided Cartesian mesh. This simplified version of the workflow has been implemented and initial test cases are starting to be run on the PISCES model and a 3D Tokamak model, as shown in Figure 1.

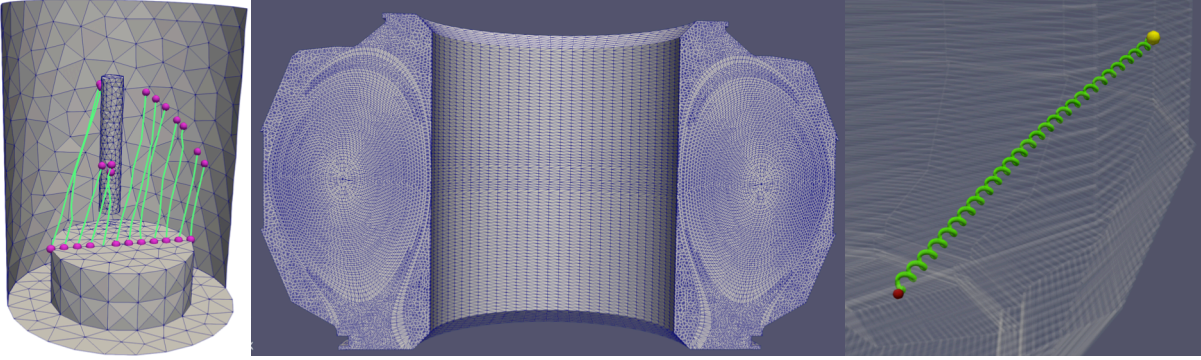


Figure 1. Tracking a small set of impurity particles in GITRm until boundary intersection using a dummy push (left), an extruded 3D mesh (center), and application of basic Boris push for a particle moving through the mesh (right).

The second type of PIC calculation is related to plasma sheath/pre-sheath region and is performed using the hPIC code. The current hPIC code employs a uniform grid. However, the plasma profile in the sheath region exhibits an exponential or boundary layer (BL) behavior, and thus, using an anisotropic boundary layer mesh based on graded and layered elements is more appropriate/efficient. Therefore, a new multi-block boundary layer mesh capability is being added in the RPI's PUMI library. This has been done to target the following three use cases in hPIC: i) 1D radial line, ii) 1D toroidal/poloidal curve, and iii) 2D scrap off layer region.

To target the desired use cases, the boundary layer mesh capability for hPIC will support three boundary layer configurations: i) one-sided BL, ii) two-sided BL, and iii) 2D multi-block BL. The mesh is represented in an implicit/logical form and mesh operations are supported using functional interfaces (APIs). Preliminary testing has been performed at the kernel level (e.g., charge density kernel) and developments are underway to fully integrate this multi-block BL mesh capability in the hPIC code. An appropriate parallelization strategy is under discussion, and will be implemented in year 3 of the project.

Uncertainty Quantification Activities modeling Impurity Transport in GITR: We have previously fit input profiles of plasma density and temperature using processed data from Langmuir probe measurements. After several variants of parametric forms, we have converged to exponential-of-polynomial forms for both the data mean and its standard deviation. Bayesian inference was performed to infer the coefficients of these polynomials, using an approximate likelihood measure that compares the probability density

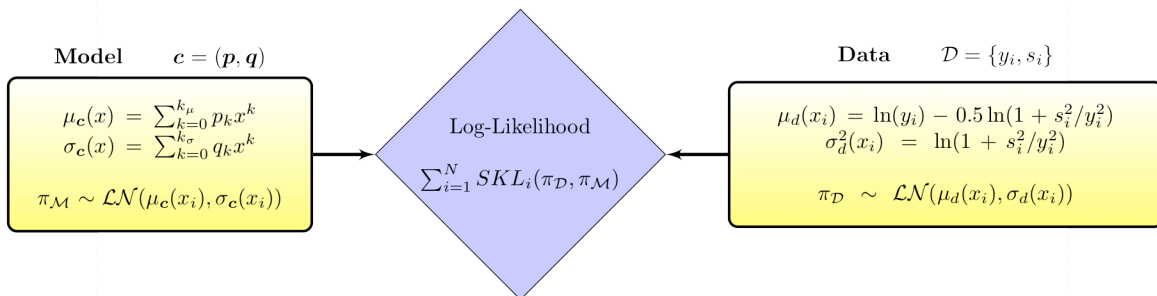


Figure 2. Details of model-vs-data comparison with a log-normal assumption and symmetrized KL log-likelihood.

functions (PDFs) of data and the model using symmetrized Kullback-Leibler (SKL) divergence, under a log-normal assumption, as illustrated by the schematic in Figure 2.

The resulting jointly-uncertain polynomial coefficients are then represented via polynomial chaos (PC) expansions. These expansions, together with the intrinsic standard deviations of the data, produce final PC representations of the two input profiles. PC representations are well-suited for non-intrusive propagation of uncertainties via general black-box models, allowing variance-based decomposition and, consequently, uncertainty attribution of outputs of interest. Specifically, input profiles' parameterization (i.e. respective PCs) were sampled and fed through the GTR code. The resulting output samples were then used to construct a PC representation for a set of outputs, including mass gains and emission. Figure 3 illustrates the result of the propagation, together with processed experimental data. We are currently investigating the reasons behind the discrepancy of GTR predictions and the respective data. Similar UQ activities are currently underway to further evaluate uncertainty in the PISCES linear plasma device exposure experiments.

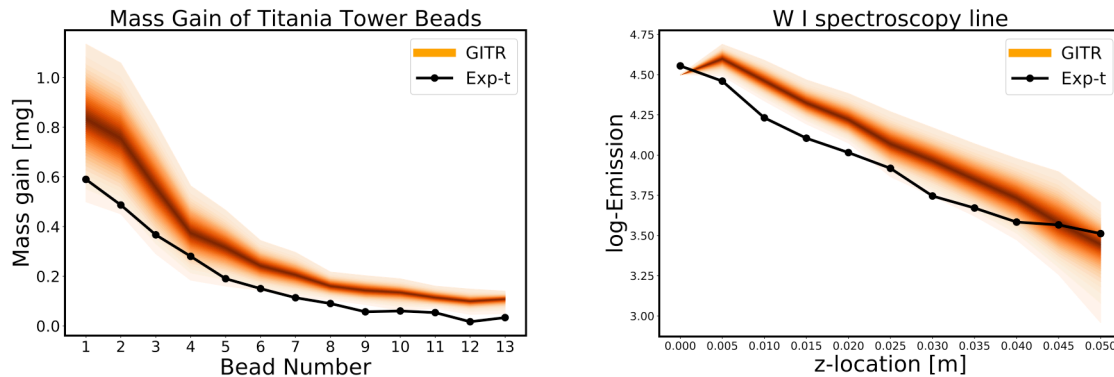


Figure 3. GTR predictions of tungsten transport and deposition in PISCES measurements (left) and the spatially dependent W spectroscopy (right) with uncertainty represented via shaded quantiles.

Sensitivity analysis in Xolotl: Monte Carlo based sampling for estimating the global sensitivity indices (i.e., fractional contributions to the variance in the quantity of interest) has been initiated within the Xolotl cluster dynamics code for simulating plasma surface interactions. This initial study, as highlighted in Figure 4, has begun to evaluate the influence on variations in the helium interstitial cluster diffusivity that impact the retained quantity of helium in tungsten surfaces. This initial study is in the process of being expanded to fully evaluate the influence of helium – hydrogen – defect interaction reaction rates on the helium bubble and hydrogen isotope concentrations.

The analysis revealed two dominant helium cluster diffusivities that impact the prediction of total helium content as predicted by the simulation. The estimates of the remaining sensitivity indices exhibited smaller magnitudes, but a convergence study was required to assess the accuracy of the estimates and confirm the result. Due to the computational expense of generating further samples for assessing convergence, a complementary analysis was performed on a subset of the original Xolotl runs using polynomial chaos (PC) based surrogate construction which delivers automatic access to estimates of the uncertainty coefficients while improving accuracy somewhat through an implicit smoothness approximation delivered by the polynomial mapping construction. Estimating these sensitivities using a least-squares regression approach delivered consistent results to the previous analysis using a fewer number of samples. A subsequent analysis using sparse regularization of the least-squares cost function was performed using Bayesian Compressive Sensing (BCS), to naturally discover a sparse estimate of the sensitivity index vector, as shown in the right panels of Figure 4, and further confirmed the dominance of the two parameters identified previously.

Xolotl diffusion parameter	Range	Gaussian
1He1	0.11-0.25	0.15+-0.05
2He2	0.2-0.3	0.25+-0.05
3He3	0.25-0.4	0.3+-0.05
4He4	0.15-0.5	0.2+-0.05
5He5	0.1-0.2	0.12+-0.025
6He6	0.3-0.45	0.4+-0.05
7He7	0.3-0.45	0.4+-0.05
8V1	1.1-1.5	1.3+-0.1

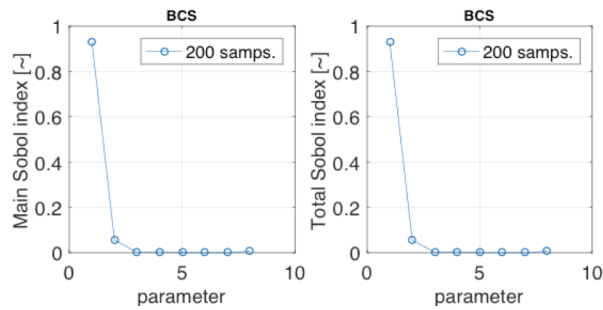


Figure 4. Specifying the range of helium diffusion coefficient (activation energy) uncertainty (left), and corresponding sensitivity indices estimated using Polynomial Chaos Expansion fitting with Bayesian comprehensive sensing, considering 8 parameters and that clearly identify 2 active parameters.

Improved Solvers for COGENT: Problems being addressed in this project are motivating the development of new capabilities in COGENT. While initial COGENT validation studies assumed adiabatic and other reduced electron models, the ability to include fully kinetic electron models is essential for the study of ELM heat pulses as described in the discussion of Task 3. The very fast time scales resulting from such models pose a significant computational hurdle that we have been working to address.

In anticipation of this and future demands on COGENT related to time-scale issues, we elected to systematically develop and implement a general and flexible time integration framework based on an additive Runge-Kutta (ARK) strategy. In the ARK approach, a system to be solved is viewed as a set of ordinary differential equations with a right-hand side composed of a sum of terms. Each term is identified as explicit or implicit, depending upon some assessment of the time scales each contains. During the time integration, the advancement of the solution due to the implicit terms involves the solution of multiple nonlinear systems, for which COGENT employs a Newton solve involving a preconditioned Krylov solve of the Jacobian system. The construction and solution of a good preconditioner is essential for the effectiveness of this approach. If preconditioners can be identified for each implicit term, an operator-split preconditioner for the entire system can then be constructed multiplicatively in terms of the individual preconditioners. If it is known that the implicit right-hand side terms act upon non-overlapping subspaces, a simpler additive form of the preconditioner can be found. COGENT now provides support for both options and some combination of them.

In applying this strategy to kinetic electron models, we are focusing initially on the treatment of fast parallel advection along magnetic field lines. Although the physics of pure advection along field lines could hardly be simpler conceptually, the properties of the associated discretized operator in the context of a preconditioned linear system solve are less obvious. For example, can a preconditioner based on an analytically integrated advection term be effective for the fourth-order, finite-volume spatial discretization of the Vlasov operator in the COGENT kinetic electron model? We are currently investigating this question using the COGENT ARK framework with the goal of significantly increasing the efficiency of the ELM heat pulse simulations.

Task 1. PFC Surface Response (Scale-bridging to extend capability of Xolotl PFC Simulator)

Implementation and testing of Be-W potentials: We have previously described our approach for generating a machine learned Spectral Neighbor Analysis Potential (SNAP) interatomic potential for modeling the tungsten-beryllium system. Interatomic potentials are an integral part of molecular dynamics (MD) simulations and will influence the accuracy of the results produced as well as provide a

multiscale link between density functional theory (DFT) and MD. There has been much recent work in attempting to create quantum-accuracy potentials using machine learning and SNAP is one such method. In the last year, we have applied the SNAP approach to the tungsten-beryllium system, where there is a lack of interatomic potentials and an interest in better understanding the interaction of beryllium in the tungsten divertor, namely the formation of W-Be intermetallics that have been observed in experiments [2]. Previously, a large database of tungsten and beryllium DFT configurations were generated as training data and a SNAP potential was fit to this data. Initial testing of the potential showed that the potential well reproduced a variety of material properties such as elastic constants, cohesive energies, and defect formation energies. We have now tested the potential against extrapolated properties that were not included in the training set and are pertinent to modeling plasma material interactions [3].

The extrapolation testing involved a series of single beryllium ion implantations in tungsten in order to generate a depth distribution profile. Determining the implantation depth of beryllium and initial interaction with the tungsten matrix provides insight into long-term beryllium diffusion and damage mechanisms. A total of 5,000 individual implantations of 75 eV beryllium into a 6 nm x 6 nm x 12 nm tungsten slab with a (100) surface orientation at 1000 K were performed. Additional implantations were performed using the binary collision approximation code Stopping Range of Ions in Matter (SRIM) [4] for comparison. The depth profiles are depicted in Figure 5 where red and blue represent MD using SNAP and SRIM respectively. The SNAP potential predicts the beryllium to remain within 20 Å of the surface, with as much as 12% residing at or above the surface. While the depth profile is slightly deeper for SRIM than SNAP, in both cases none of the beryllium penetrates more than 30 Å below the surface. Both results indicate a strong preference for beryllium to implant close to the surface, having a much shallower depth profile than either hydrogen or helium at this energy.

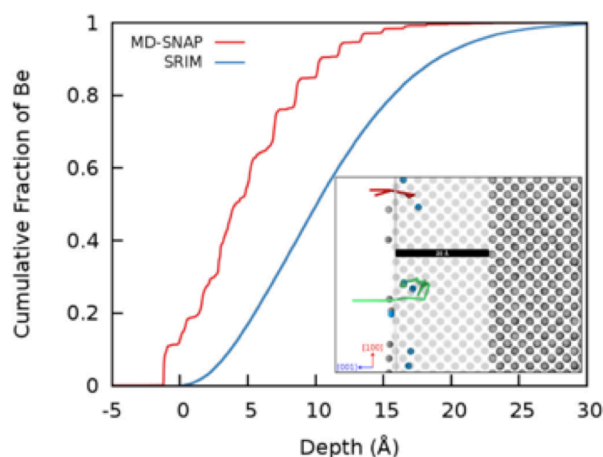


Figure 5. Plot of cumulative depth distribution of 75 eV Be in tungsten at 1000 K using both MD (red) and SRIM (blue). Inset displays an atomistic snapshot of the Be (blue spheres) implanted onto the (100) surface of tungsten (grey spheres). The red/green trajectory lines show the time history of a rejected/captured Be atom, respectively.

Further work has been performed to model cumulative beryllium implantation in tungsten. Two sets of simulations have been performed, beryllium implantation into tungsten at 75 eV and athermal beryllium deposition onto the tungsten surface. In both cases, the simulations were performed at 1000 K with a 6 nm x 6 nm x 12 nm tungsten slab with a (100) surface orientation and the total simulated time was 50 ns. Significant mixing of tungsten and beryllium into an amorphous layer is observed in both cases and is limited to the very near surface region with beryllium remaining entirely within the first 2 nm of the material. An exchange mechanism was observed that allows tungsten to diffuse from the bulk into the mixed layer. While the mixed layer appears amorphous, further analysis indicates a trend towards an hcp like structure. These simulations have been recently expanded to include the (110) and (111) surfaces. In these cases, ordered structures have been observed after either beryllium implantation or deposition, especially for the (111) surface. The ordered structures are similar to the expected phase of WBe₂, one of the stable intermetallics that has been observed in experiments. These initial results can provide insight into the early stages of intermetallic formation. Further work and analysis is needed to reach longer simulation times to study the evolution of these surface layers over time and to determine mechanisms for the formation of these mixed layers.

In addition to the current W-Be work, we are expanding the SNAP potential to include hydrogen. Recently, a database of hydrogen DFT training data that adds an additional 15,000 configurations has been generated and includes data for pure hydrogen as well as hydrogen in tungsten and beryllium. The database includes a variety of configurations such as hydrogen at surfaces and defects in tungsten and beryllium as well as atomic and molecular hydrogen binding energies. Current work involves fitting both the SNAP potential hyperparameters as well as training group weights, with the goal of generating a consistent W-Be-H SNAP potential.

Large-Scale MD Simulations of H diffusion and interaction with He bubbles in tungsten: Large-scale MD simulations are in progress to investigate helium-hydrogen interactions in plasma exposed tungsten at NERSC, ALCF and OLCF. This section briefly describes results of evaluating two different tungsten-hydrogen (W-H) interatomic potentials. One is an embedded atom method (EAM) [5], while the other is a more computationally expensive many-body Tersoff-style potential, initially fit by Juslin [6], but later modified by Guterl [7]. This Tersoff-style potential is roughly 30 times slower than the tungsten-tungsten (W-W) potential used in tungsten-helium (W-He) simulations previously reported, but our use of GPUs can reduce the simulation time by a factor of 2-3, and current work has focused on further optimizing the GPU performance of the Tersoff-style and SNAP potentials. Figure 6 shows the time dependence of the hydrogen concentration profile evolution following the insertion of a layer of highly concentrated hydrogen at a depth of 9–10 nm below the surface containing a distribution of pre-existing helium bubbles. In Figure 6, the zero-depth position is used to define the initial hydrogen layer; negative values indicate hydrogen diffusion toward the top surface, and positive values indicate deeper hydrogen diffusion. The evolution of these concentration profiles can be used to assess the hydrogen diffusion coefficient to determine the impact of the helium layer.

From Figure 6, it is also readily apparent that hydrogen is predicted to diffuse faster by the EAM than with the Tersoff potential, as seen by the much more rapid decrease in hydrogen concentration as the profile broadens significantly. It is also notable that the EAM potential indicates that much more hydrogen reaches the top surface within several nanoseconds, but the Tersoff potential does not predict comparably rapid hydrogen segregation to the surface. Both potentials predict that helium will significantly slow the hydrogen permeation (compared with a similar set of simulations performed without the initial helium bubble layer), with resulting hydrogen diffusivity values that are 6–10X less when diffusing through the helium bubble layer than diffusing through nominally pure tungsten. The significant reduction in hydrogen diffusion through the pre-existing helium bubble layer is the result of two significant interactions: First, hydrogen tends to form relatively strongly bound cluster configurations with the small helium clusters and larger bubbles; and Second, the helium bubble layer below the tungsten surface induces biaxial compressive stress in the tungsten lattice, and this local stress state also significantly influences the hydrogen diffusion characteristics.

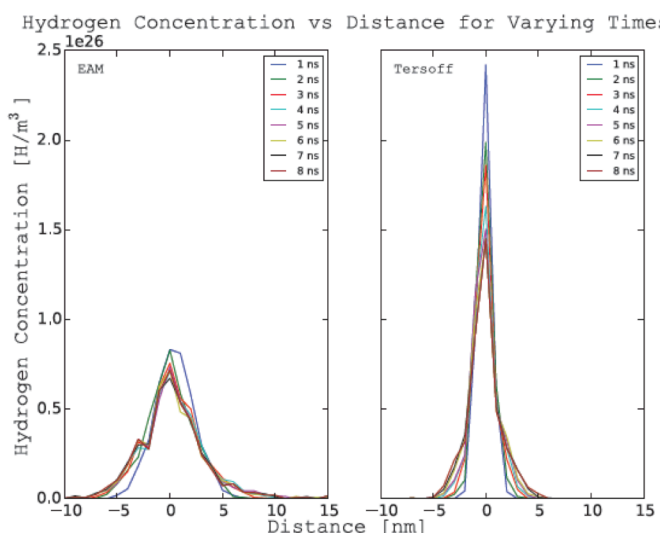


Figure 6. Subsurface hydrogen concentration evolution following implantation into a subsurface helium bubble distribution in tungsten as a function of time, using an EAM (left) or Tersoff (right) W-H interatomic potential.

Effects of sub-surface helium on the elastic properties of tungsten: Studying the impact of helium (He) ion implantation on the thermomechanical properties of tungsten is of utmost importance for evaluating

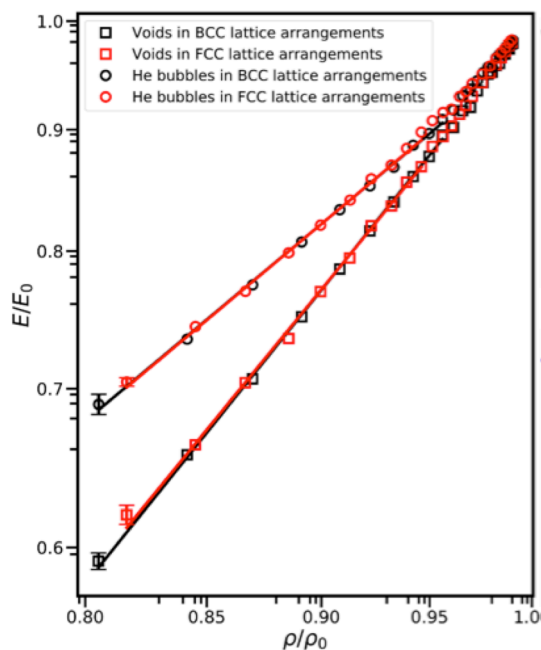


Figure 7. MD computed elastic modulus, E , as a function of atomic density, ρ , of damaged tungsten containing a periodic array of spherical cavities with radius of $4a$ at 1000K; E_0 , ρ_0 and a are the modulus, density and lattice parameter, respectively of perfect tungsten. The solid lines are power-law fits to the MD results.

tungsten as a plasma-facing component (PFC) in nuclear fusion devices. Toward this end, we have conducted systematic MD computations of the elastic modulus of single crystalline tungsten containing voids (nanopores); filling these nanopores with the proper amount of He to form helium nanobubbles, as derived by analysis of large-scale MD simulations of the structural evolution of He-implanted single crystalline tungsten [8], has been used to generate models of plasma-exposed tungsten and to assess the effect of He-ion irradiation on tungsten's elastic properties. We have conducted a systematic exploration of the relevant parameter space: the parameters varied include porosity (tungsten matrix density), temperature, helium bubble radius, arrangement of helium bubbles in regular arrays, and helium content. Our computations reveal that the dependence of the elastic modulus of nanoporous tungsten on its density follows a power-law scaling relation, as shown in Figure 7, similar to that of the modulus-density relations of natural cellular materials. We find that arrangement of voids/bubbles in various lattice configurations in the tungsten matrix does not have any important effect on the elastic modulus, as seen in Figure 7. We also find that filling the nanopores with helium increases the stiffness of PFC tungsten and decreases the sensitivity of its stiffness to porosity.

At a given temperature, we find that decreasing He nanobubble size leads to stiffening of PFC tungsten and reduces the sensitivity of its stiffness to porosity. Moreover, we find that at given nanobubble size, raising the temperature leads to relative stiffening of PFC tungsten, with respect to the stiffness of perfect tungsten at each temperature, and reduces the stiffness sensitivity to porosity. Finally, our computations demonstrate a substantial softening of the elastic modulus of plasma-exposed tungsten with increasing He content in the PFC tungsten matrix, with this softening effect becoming stronger with increasing size of helium nanobubbles. Our findings enable the development of a quantitative database for the elastic modulus dependence on He content in PFC tungsten at various plasma exposure conditions, which constitutes another important component toward modeling and simulation of PFC surface morphological evolution.

Helium and Hydrogen diffusion along dislocations: Crystal defects in Tungsten (W), such as grain boundaries and dislocations, can serve as traps and channels for diffusion of Hydrogen (H) and Helium (He), which might modify the retention propensity of the plasma facing material leading to undesirable consequences. We have studied the diffusion of H, He, and self-interstitial atoms (SIA) inside screw and edge dislocations in W using Molecular Dynamics (MD) simulations with a recently developed EAM interatomic potential [5]. From an energetic perspective, interstitial atoms would likely favor sites with largest free-volume. Evident from Figure 8(a) is the presence of interconnected regions of large free-volume resulting in 'channels' inside the core of the edge dislocation. Such inter-connected regions are not present in the screw dislocation (Fig. 8(b)). The distribution of free-volume indicates that interstitial

atoms can undergo 1-D diffusion in these channels in the edge dislocation. In the screw dislocation, the regions of maximum-free volume are present as ‘lobes’ with nominal 3-fold symmetry around the core of the screw dislocation.

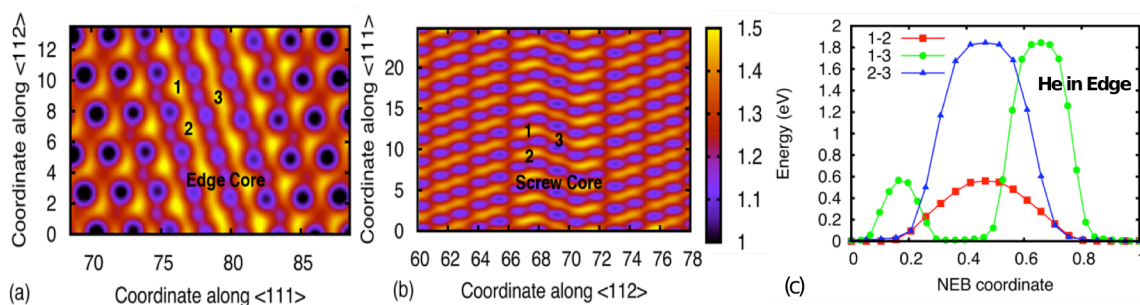


Figure 8. 2D projection of the free-volume contours on the mean-plane of the dislocation core. (a) Edge dislocation (b) Screw dislocation. Numbers 1,2,3... are used to denote the sites with maximum free-volume where interstitials are positioned for NEB calculations. (c) Energy of NEB replicas as a function of the reaction coordinate for site-to-site hopping of He inside the edge dislocation core.

Following the identification of stable sites, we performed nudged-elastic band (NEB) [9] calculations to determine the energy barrier for site-to-site migration of interstitials. The curve denoted as 1-2 in Figure 8c shows the energy of the NEB replicas for site-to-site hopping of He within the channel at the edge dislocation core, with a predicted energy barrier of 0.56 eV. A much higher barrier of 1.84 eV is predicted for direct hopping from one channel to another (2-3). The curve denoted as ‘1-3’, which is also for channel-to-channel hopping, shows two barriers: a smaller barrier of 0.56 eV for in channel hopping from site 1 to site 2, followed by the larger barrier of 1.84 eV for channel-to-channel hopping from 2 to 3 (Fig. 8a)). Therefore, the smallest barrier predicted for He diffusion inside the edge dislocation core is 0.56 eV. On the other hand, NEB calculations reveal that hopping from lobe-to-lobe (1-2 in Fig. 8b)) in the mean-plane of screw dislocation has a high energetic barrier > 2.5 eV for both He and H. At the same time, lobe-to-lobe hopping along the helix of the screw dislocation has relatively low barriers of 0.70 eV for He and 0.86 eV for H. In addition, it can be seen that He and H can move from the interior of the screw to the lobes (3-1) with very small barriers of 0.05 eV for He and 0.07 eV for H. Qualitatively, this agrees with previous DFT [10] calculations that have predicted energy barriers ~ 0.07 -0.1 eV for migration of H between meta-stable sites on screw dislocation. Based on these results, it can be deduced that diffusion of H and He along the core of the screw dislocation does not happen and lobe-to-lobe hopping along the helix of the screw dislocation core is the most probable mechanism for diffusion of H and He. These results indicate confined 1D transport of H and He at the edge dislocation core, which leads to coupled He/H transport with dislocation motion, and that H and He will also have 1D diffusion along the helix of a screw dislocation core, but in both cases, higher activation energies for diffusion are obtained in comparison to the bulk.

Experimental investigations of tungsten fuzz: We initiated experiments in PISCES-A to enable a comparison to the modeling results. The experiments involved rapidly varying the bias voltage to a target, and thereby the incident ion energy and heat flux. The idea was to measure the change in light emission directly in front of the sample due to thermal outgassing from the change in sample temperature. Unfortunately, changing the incident ion energy also changed the secondary electron emission from the sample and this change dominated changes to the plasma light emission and so the measurement of outgassing was unsuccessful. We are presently working to redesign the experimental conditions and will attempt the experiment once this is complete. As well, a series of measurements were performed to provide data on surface mobility and material migration. These measurements used thin tungsten layers deposited on molybdenum targets to examine the possible migration of material due to nano-bubble formation at lower sample temperature. After helium plasma exposure the surface composition and depth

profiles of the layer and substrate materials were obtained. These experiments did not provide evidence of migration of the substrate through the thin layers at low temperature. However, at 1000 K, the Mo substrate atoms appear at the surface. At this temperature the surface did not yet develop a fuzzy structure, but material migration is already evident. In the future, specific simulations will target the experimental conditions to provide experimental validation of the SciDAC models.

Continuum-level modeling of the origin of fuzz formation: Helium (He) implantation in tungsten (W), the plasma-facing material (PFM) candidate for the divertor in nuclear fusion reactors, develops a fuzz-like surface morphology under typical reactor operating conditions, namely, over the temperature range from 900 K to 2000 K and above a threshold incident ion energy of approximately 20 eV. This fragile ‘fuzz’ surface nanostructure adversely affects reactor performance and operation. Toward a fundamental understanding of the growth of this extremely complex nanostructure on the surface of PFM tungsten, we have developed a predictive model of the initial stage of fuzz formation, capable of simulating the spatiotemporal scales relevant to the fuzz formation process placing emphasis on the onset of fuzz formation.

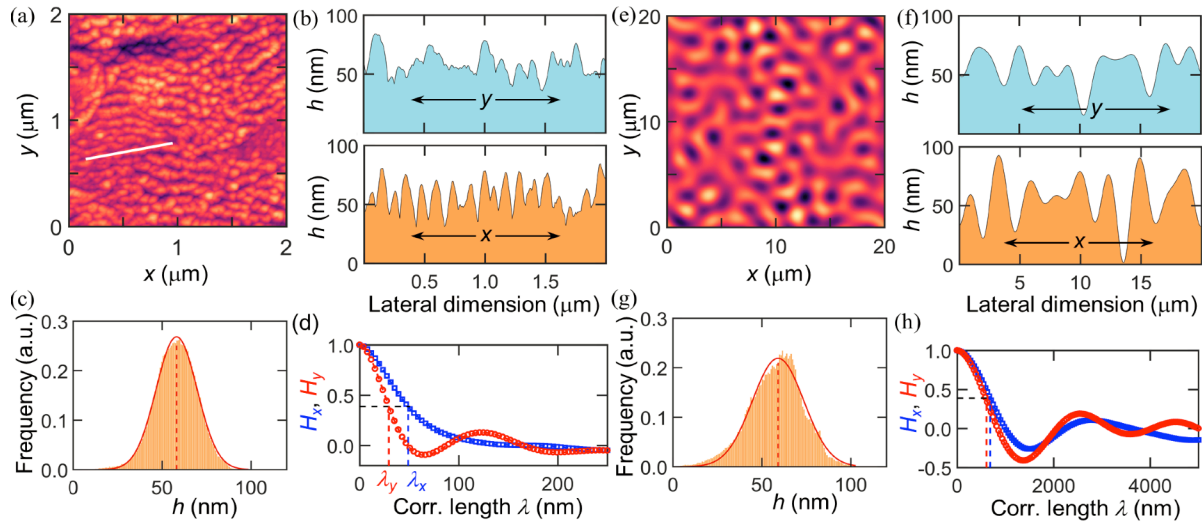


Figure 9. Comparison of model-predicted surface morphology of plasma-exposed tungsten (right) with experimental measurements (left) after 80 minutes of exposure to 75 eV helium. (a,e) Top view of surface morphology, (b,f) cross-sectional view of the surface profile, (c,g) surface height distribution function, and (d,h) surface height autocorrelation function.

This atomistically-informed, continuous-domain model describes the surface morphological evolution of helium-ion-irradiated tungsten. The constitutive equations of the model are parameterized using large-scale molecular-dynamics (MD) simulations [8]. The helium nanobubble region below the plasma-exposed tungsten surface is modeled as a strained thin homogeneous layer with uniform nanobubble size and number density, while the bulk tungsten is not actively participating in the fuzz formation process and is modeled as a semi-infinite rigid substrate. The nanobubbles are assumed to be spherical, the He/W matrix interfacial tension is assumed to be isotropic, and the material properties of the nanobubble region are taken to be the same as those of bulk tungsten. The relation between the number of He atoms and the number of vacancies in the nanobubbles is based on MD simulations [8] and is used to determine the pressure in the nanobubbles. For the He-implanted W layer (nanobubble region), the stress level due to the over-pressurized He bubbles is calculated using heterogeneous elastic inclusion theory and the state of stress in this region is taken to be equibiaxial compressive. The assumptions for the stress state and the

corresponding stress level are validated based on MD simulations of the deformation state of a He-implanted W region. Finally, instead of loop punching, an interstitial flux to the surface is considered.

Based on the above model, we have conducted self-consistent numerical simulations of the dynamics of the He-implanted W surface morphology and, for model validation purposes, we have also carried out systematic comparisons of the simulation results with measurements from carefully designed experiments of tungsten He-plasma irradiation followed by structural and morphological characterization of the plasma-irradiated samples. Under the experimental conditions of a medium-flux RF plasma source ($\sim 3 \times 10^{20} \text{ m}^{-2}\text{s}^{-1}$) exposure of 75 eV He on ITER-grade W at 1113 K, the predicted surface morphology shows a good qualitative and quantitative agreement with experimental data after a He plasma exposure time of 80 min, as shown in Figure 9. The strong quantitative agreement between the mean and width of the height distribution functions for the experimental and computed W surface morphologies establishes that our model can successfully predict the initial growth rate of nanotendrils emanating from the surface, which is the precursor to fuzz formation. A parametric sensitivity analysis for the effects of two key model parameters, the He concentration in the He-implanted tungsten and the He nanobubble size, on our model predictions for the average nanotendril spacings and the nanotendril growth rate shows that the features of the He-plasma-irradiated tungsten surface depend weakly on nanobubble size at low He fluence but the dependence becomes much stronger at high He fluence.

KMC-MD studies to predict structure evolution and properties: This activity aims to predict microstructure and property evolution of plasma-facing materials exposed to particle bombardment from the plasma, including neutrons, under isothermal and variable temperature conditions. To investigate PFC structure-property relations, a combination of atomistic simulations is performed. These simulations include density functional theory (DFT) calculations, molecular dynamics (MD) simulations using reliable interatomic potentials for tungsten-based materials, and object kinetic Monte Carlo (OKMC) simulations. This activity involves a close collaboration with the University of Massachusetts, Amherst (for the DFT and MD work). Over the past year, the effort has focused extensively on benchmarking the OKMC simulations, the results of which are not shown here in the interest of brevity. Once the task of benchmarking is complete, we intend to carry out OKMC simulations to study the long-time near-surface microstructural evolution in tungsten under isothermal conditions. Sensitivity analysis is useful in determining parameters to which the system output is most responsive and in assessing the robustness of the system to extreme circumstances or unusual environmental conditions. Therefore, we intend to study the He accumulation as function of surface orientation and He flux ($10^{21} - 10^{24} \text{ He m}^{-2}\text{s}^{-1}$) before proceeding to the simulations of He accumulation under variable temperature conditions caused by ELMs (Edge-Localized Modes). The initial set of simulations under variable temperature conditions would be limited to square like ELM pulses corresponding to 0.5 MJ m^{-2} energy deposited with a pulse width of 0.5 ms, and will be reported in future reports.

Year 3 focus: The Task 1 activities for year 3 will continue along the originally identified plan, with the addition of work to evaluate the opportunity for fitting a machine learning SNAP potential for W-N, and continue the focus on extending predictions of helium bubble induced microstructures to the thermal-mechanical property response of tungsten PFCs. The focus of our large-scale MD simulations are transitioning to evaluating hydrogen simulations to evaluate mechanisms related to hydrogen interaction and trapping at extended defects such as voids and grain boundaries, and to identify mechanisms associated with helium and hydrogen interactions with mixed beryllium – tungsten surfaces for implementation in our continuum scale cluster dynamics code Xolotl. The accelerated MD simulations are focused on identifying the mechanisms of helium bubble coalescence and on evaluating helium bubble effects on grain boundary mobility to assess the impact of helium on tungsten re-crystallization kinetics, which is a priority for ITER. Xolotl simulations within the integrated PMI modeling framework will begin focusing on experiments being performed on WEST, as well as benchmarking against PISCES experiments.

Task 1 researchers will continue the strong engagement with CS/AM researchers to incorporate UQ methodologies to identify the most sensitive parameters controlling predictions of helium and hydrogen concentrations in tungsten PFCs, and to engage with the PETSc team for optimization of the solvers and pre-conditioners in Xolotl.

Task 2. Integrating boundary plasma and PFC Surface models to predict PFC Performance

The majority of activities within Task 2 this year have focused on successful completion and delivery of the DOE Office of Fusion Energy Sciences FY2018 Performance Measure Management (PMM) reportable milestone in Fusion Theory and Simulation, which involves modeling Plasma Materials Interaction (PMI). Since this document is now publicly available [1], we will not reproduce the report here. One significant activity within Task 2 that is described within this report is the modeling of the tungsten metal rings campaign performed in DIII-D.

Modeling and analysis of tungsten source and transport in DIII-D divertor: Experiments conducted during the Metal Rings Campaign in DIII-D were modeled and analyzed to examine tungsten sourcing and transport in tokamak divertor. This initial modeling activity has used the ERO-D3D code, but we anticipate future effort using GITR. First, the exposure of a toroidally symmetric tungsten ring inserted in the lower outer divertor of DIII-D to 25 repeated, attached L-mode shots in reverse-Bt configuration has been modeled [11]. Plasma background conditions were obtained from the 2D transport code UEDGE. Tungsten and carbon erosion, transport and deposition in the DIII-D outer divertor were modeled with ERO-D3D, a high performance computing version of the ERO code. Radial profiles of the W gross erosion flux inferred in-situ from spectroscopic measurements of the WI line (400.9nm) during these experiments were well reproduced by ERO-D3D simulations of carbon and tungsten impurity erosion, transport and redeposition in the outer divertor region, as shown in Figure 10. For plasma conditions with an attached divertor in DIII-D, tungsten gross erosion was shown to be mainly induced by physical sputtering of tungsten by carbon impurities.

The analysis of low-Z impurity transport in the DIII-D outer divertor indicated that the outward radial transport of carbon impurities in the outer divertor is mainly governed by ExB drifts in the sheath region. It was also demonstrated that the erosion and redeposition of carbon on tungsten, induced by the implantation of carbon into tungsten modeled with the homogeneous mixed material model, increases the effective flux of carbon impurities onto the tungsten ring (carbon recycling on tungsten). Moreover, the localized deposition of tungsten measured experimentally in the outboard region away from the tungsten ring was shown to be caused by the long-range radial transport of tungsten impurities in the outer divertor region induced by the interplay between poloidal and radial ExB drifts outside of the sheath region. This modeling and analysis of carbon and tungsten erosion and redeposition eventually demonstrates that various physical mechanisms and their synergistic effects, such as ExB drifts inside and outside of the sheath region and low-Z impurity

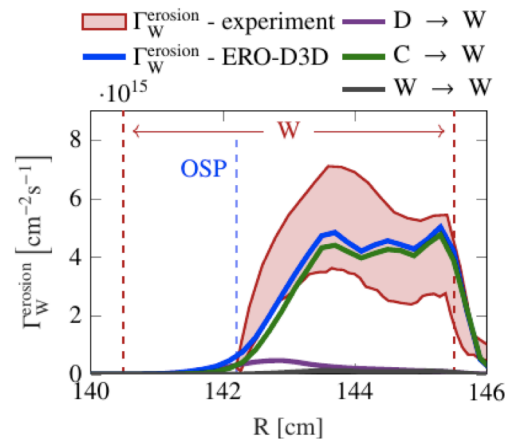


Figure 10. Experimental (red area) and simulated (blue) tungsten gross erosion flux as a function of the radial location in the DIII-D divertor. Contributions of carbon impurities (green) and tungsten impurities (gray) to tungsten sputtering are shown, as reproduced from Ref. [11].

recycling in divertor, need to be taken into account to accurately describe erosion, transport and redeposition of impurities in tokamak divertors.

The toroidally symmetric tungsten ring inserted in the lower outer divertor of DIII-D was also exposed to various H-mode plasmas [12]. These experiments were modeled and analyzed to examine the relationship between the tungsten gross erosion and the ELM characteristics. The OEDGE code was used to model plasma background conditions and carbon erosion, transport and redeposition between ELMs. The one-dimensional ‘free-streaming’ ELM model was used to model plasma conditions during ELMs. A carbon-tungsten mixed target material was used for both inter-ELMs and intra-ELMs simulations, and tungsten gross erosion was estimated using a simple analytical TRIM.SP sputtering model. Within this framework, it was shown that the inter-ELM tungsten gross erosion rate is not sensitive to the carbon fraction on the tungsten surface, and wider range of carbon fractions from 0.3 to 0.6 give similar tungsten gross erosion profiles and match the diagnostic data, in agreement with a simple analytical model. On the other hand, intra-ELM simulations indicated that the carbon fraction must be around 0.3 to reproduce the tungsten gross erosion flux measured spectroscopically, as shown in Figure 11. For both inter- and intra-ELM cases, carbon was shown to dominate the tungsten erosion. Finally, it was shown that the inter-ELM tungsten erosion is dominated by locally redeposited carbon, as in L-mode plasma conditions, whereas the energetic high charge state carbon impurities originating from the pedestal can significantly contribute to the substantial tungsten erosion in the near-separatrix region during ELMs (see Fig. 11).

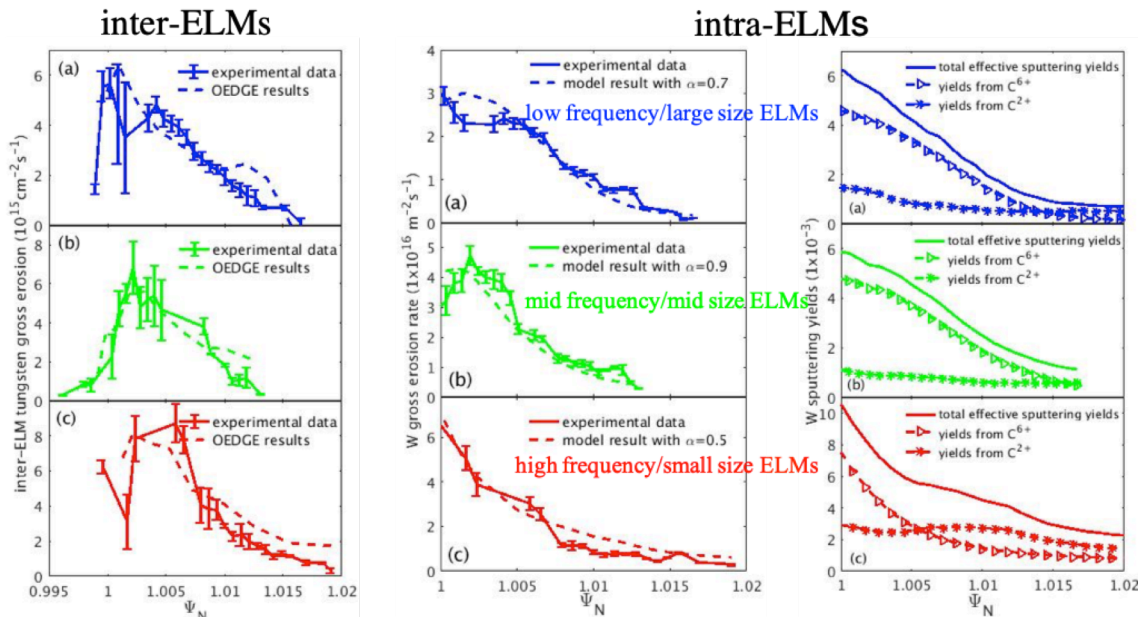


Figure 11. Simulated and experimental tungsten gross erosion profiles between (left column) and during ELMs (middle column), and contributions from energetic C^{6+} ions and locally re-deposited C^{2+} to W sputtering during an ELM (right column). The carbon fraction on the tungsten surface has been set to 0.3, as reproduced from Ref. [12].

The net erosion of W PFCs in tokamak divertor is the convolution of W gross erosion and W re-deposition, and thus ultimately determines the effective sources of W in tokamak divertor. Unlike tungsten gross erosion, tungsten net erosion cannot be monitored during plasma operations using spectroscopic measurements. Robust modeling of tungsten net erosion is thus required to predict tungsten source in the SOL plasma. To that end, mechanisms governing tungsten net erosion were investigated using ERO-D3D to assess the robustness of a W net erosion predictive model [13].

The validity of the model describing tungsten prompt redeposition can be examined using tungsten net erosion measurements obtained during several dedicated experiments in DIII-D divertor. To that end, a reduced model of high-Z impurities erosion and redeposition was developed to analyze net erosion of high-Z material in divertor attached plasma conditions measured in DIII-D experiments [14]. This reduced model is tailored to quantify the redeposition and the net erosion on high-Z material samples of sufficiently small dimensions to be considered exposed to uniform plasma conditions. For those uniform plasma conditions, the spatial distribution of redeposited high-Z impurities was well approximated by an analytical distribution characterized by a few parameters. The fraction of high-Z impurity eroding and redepositing on a material sample was then obtained by integrating this distribution across the material sample. The ratio of net erosion rates of tungsten measured experimentally from tungsten samples of different sizes exposed to the same attached plasma conditions were well reproduced with this reduced model. It was also shown that uncertainties induced by radially non-uniform plasma conditions in experiments can be significantly reduced by exposing samples to high density divertor plasma.

Year 3 focus: Ongoing and future activities within Task 2 will continue to focus on issues identified by the ITER Divertor and Plasma Surface Interactions Section related to evaluating the performance of a high flux expansion divertor operating in conditions of deep detachment, and beginning to simulate the maximum ELM size for which the burn-through conditions can be avoided. As well, we plan to continue to focus on the continued code development of GITR and hPIC, especially related to being able to self-consistently model the transport and evolution of neon gas injection to dissipate the divertor heat flux.

An increasing focus during the coming year will be to merge Task 2 and Task 3 researchers to accelerate progress on dynamic code coupling to address issues of the dynamic wall response and the ability to simulate PSIs during ELMs. This will involve a concerted effort to incorporate and extend the IPS workflow to handle time dependent inputs, and to provide feedback from the surface response to SOLPS. Validation efforts within Task 2 are now beginning to focus on the WEST long-pulse tokamak, and specifically targeting the helium discharge campaign C4.

Task 3. Dynamic wall response & feedback to divertor plasma

The objectives of the Task 3, co-led by Ilon Joseph (LLNL) and Sergei Krashenninikov (UCSD), are to develop predictive computational models of plasma-material interactions (PMI) for two of the most important outstanding issues:

1. material surface erosion due to transient power and particle loads, and,
2. dynamic recycling of main ions and impurity species between the plasma and wall.

In order to develop predictive capability, high-fidelity models for both the edge plasma and material PFCs must be coupled together. The goal is to perform the first studies of dynamic recycling and material erosion caused by transient events that include kinetic effects from the SOL plasma to the sheath to the material surface.

Over the first two years of the project, the focus of Task 3 has been to develop divertor-relevant kinetic and fluid plasma computational models and utilize them to dynamically predict the flux of particles and energy impinging on plasma facing components (PFCs). We are simultaneously working to improve the physics modeling and computational capabilities of the wall codes in order to become technically ready for plasma-wall coupling. In the second and third years, the main objectives are to implement and test coupling strategies for studies of materials erosion under transient conditions relevant to ELMs and to perform initial physics studies of surface evolution under transient plasma conditions. At first, we are focusing on explicit coupling strategies; implicit coupling strategies may be necessary if the coupled problem introduces fast time scales. We are developing coupling strategies by exploring the available numerical methods and by analyzing of the physics of the coupled models.

Summary of Accomplishments (Sept. 2018-June 2019):

- Implemented ELM-relevant heat pulse models within the COGENT code, including new capabilities and postprocessing methods for the Boltzmann electron model
- Explored physics of heat pulse model using kinetic ions and Boltzmann electrons, as well as kinetic ions and kinetic electrons; performed model verification studies
- Developed BOUT++ divertor-relevant turbulence model, including resistive-ballooning physics and conducting wall sheath BCs in mapped slab geometry; began implementation of neutral fluid model
- Performed a variety of linear and nonlinear divertor turbulence verification studies; initial exploration of nonlinear regimes of saturated quasi-stationary divertor turbulence
- Compared linear growth rates and saturated turbulence amplitudes in straight magnetic field geometry to validation studies of experimental turbulence on LAPD
- Formulated strategies for coupling plasma codes (UEDGE, BOUT++, SOLPS) and wall codes (FACE, Xolotl)
- Coupled UEDGE plasma code to FACE wall code using explicit coupling strategy; exploration of the physics of the coupled model for both steady-state conditions and for ELM heat pulses

Development of SOLT3D divertor turbulence model within BOUT++: We have implemented a divertor-relevant turbulence model within the BOUT++ framework, that we refer to as “SOLT3D,” and is an extension of the physics of the 2D SOLT model [15] to 3D. The SOLT3D model evolves the ion density, N_i , the electron temperature, T_e , and the vorticity (fluid version of the gyro-Poisson) to determine the electric potential, ϕ , in a simplified geometry appropriate for the divertor leg. With this equation set, the model includes the physics of the most relevant modes of turbulent instability: coupled resistive ballooning modes (RBMs) and drift waves (DRBMs). The model also includes a linearized version of sheath BCs which drives the conducting wall mode (CWM) instability, which is one of the most important modes to consider for turbulence near the divertor target plates. Linear verification tests of these modes of instability have been checked against analytic theory and past simulation models. We have also performed nonlinear verification tests for plasma turbulence in straight magnetic field geometry. We are in the process of adding a fluid model for neutrals to the equation set that will ultimately allow us to couple the model to the wall codes, such as FACE and Xolotl. The coupled code will become our primary tool for studying the interplay between dynamic recycling processes and divertor turbulence. We have added a neutral particle density, N_n , conservation equation, in addition to the ion particle density, N_i , conservation equation; the neutral temperature is assumed to equal the ion temperature due to the fast charge exchange collisions. The next phase will be to assess the impact of the neutrals on linear stability and on nonlinear plasma turbulence.

Explicit plasma-wall coupling between UEDGE and FACE: We have performed simulation studies to evaluate the impact of dynamic wall out-gassing on transient events in Scrape-off-Layer plasmas of fusion devices using the recently coupled in fully time-dependent mode edge plasma transport code UEDGE and wall code FACE. The simulations were performed in one-dimensional geometry representing a narrow magnetic flux surface in SOL region. In order to simplify analysis, the “closed box” approximation was used, where total number of particles in the system has been conserved. The simulated plasma included deuterium ions and neutrals, as well as nitrogen impurities with a non-uniform density profile set as a fixed fraction of plasma density in divertor region. The divertor target material parameters were chosen corresponding to tungsten and included single kind of hydrogen traps with de-trapping energy of 0.9 eV and uniform density of 0.1 at.%. The heat conduction equation in the wall was also solved, where wall temperature at the non-plasma exposed side was kept constant at 500 K. Both the plasma ion and the neutral fluxes to the wall were considered individually with corresponding dynamic recycling and albedo coefficients. Initially, the system was prepared in a steady state, where the recycling and albedo coefficients were equal exactly one and wall state was determined by the particle and heat

fluxes from the plasma. The transient heat load was then modeled by varying in time the plasma heating power according to prescribed ELM characteristics.

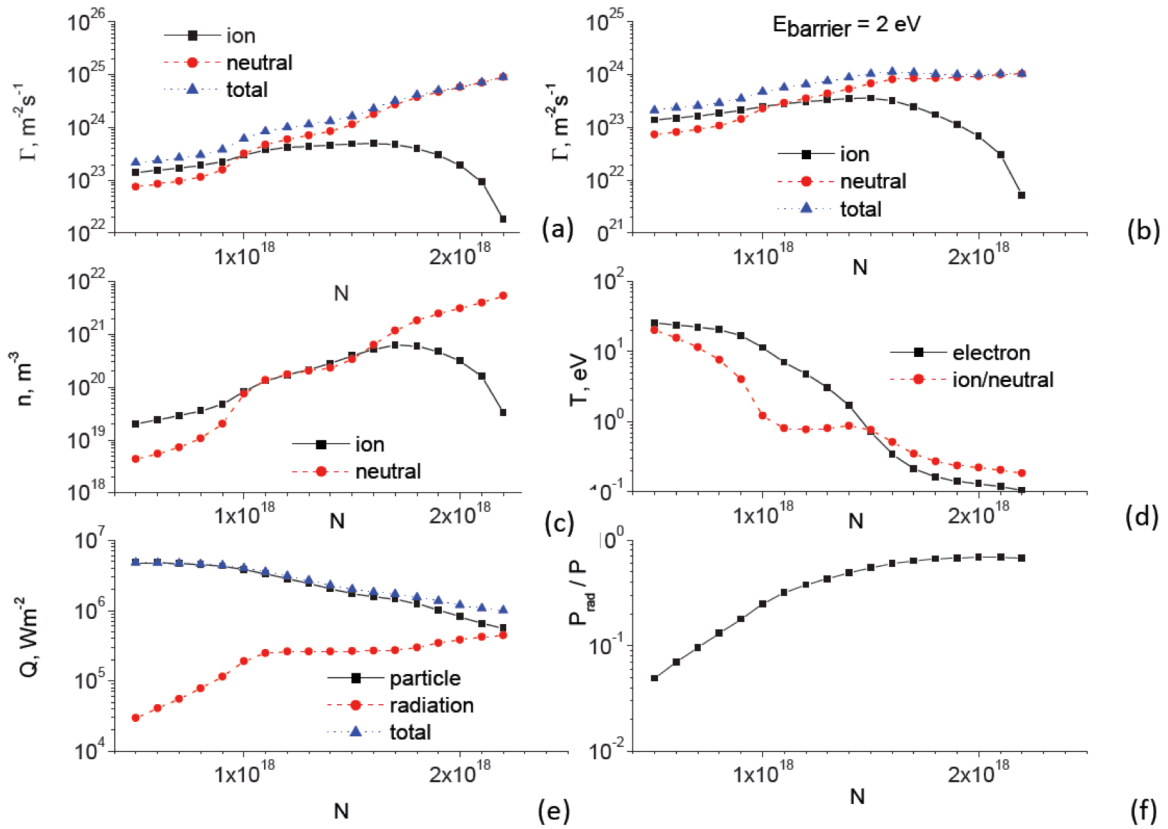


Figure 12. Dependencies of various plasma parameters on the total number of hydrogen particles in the simulated UEDGE-FACE steady state 1D system. a) particle fluxes to the wall; b) particle fluxes implanted into the wall; c) plasma density in the wall vicinity; d) plasma temperature near the wall; e) power flux to the wall; and f) total plasma radiated fraction.

We conducted a scan of the steady state plasma solutions for the different total number of plasma particles, as shown in Figure 12. This Figure demonstrates a transition from attached to deeply detached divertor plasma regimes, characterized by rollover of the ion flux to the wall as the number of particles in the plasma increases. In the detached divertor regimes, the density and flux to the wall of neutrals increases dramatically, while the wall total heat load decreases and the plasma temperature near the target drops below 1 eV. This creates conditions, where the low energy plasma particles cannot penetrate into the target material and the particle flux implanted into the wall decreases despite dramatically increased incoming flux of neutrals.

The time dependent simulations of an ELM-like heat pulse of 3 ms duration were performed for the different initial plasma regimes, and the results are shown in Figure 13. The obtained results of the transient simulations demonstrate that during ELMs heat flux to the wall increases disproportionately to the increase of the upstream heating power due to reduction of radiative power losses in divertor as plasma temperature there transiently increases. That leads to a substantial increase of divertor target temperature and net release of large amounts of hydrogen from the target material due to thermally activated detrapping. The simulations demonstrate that net hydrogen release can occur even as the implanted hydrogen flux from the plasma increases significantly during an ELM. These simulated results

demonstrate the importance of plasma-wall coupling considerations, and begin to evaluate the coupling methodologies and timescales for future implementation in the codes used in the FY2018 Fusion Theory and Simulation PSI milestone.

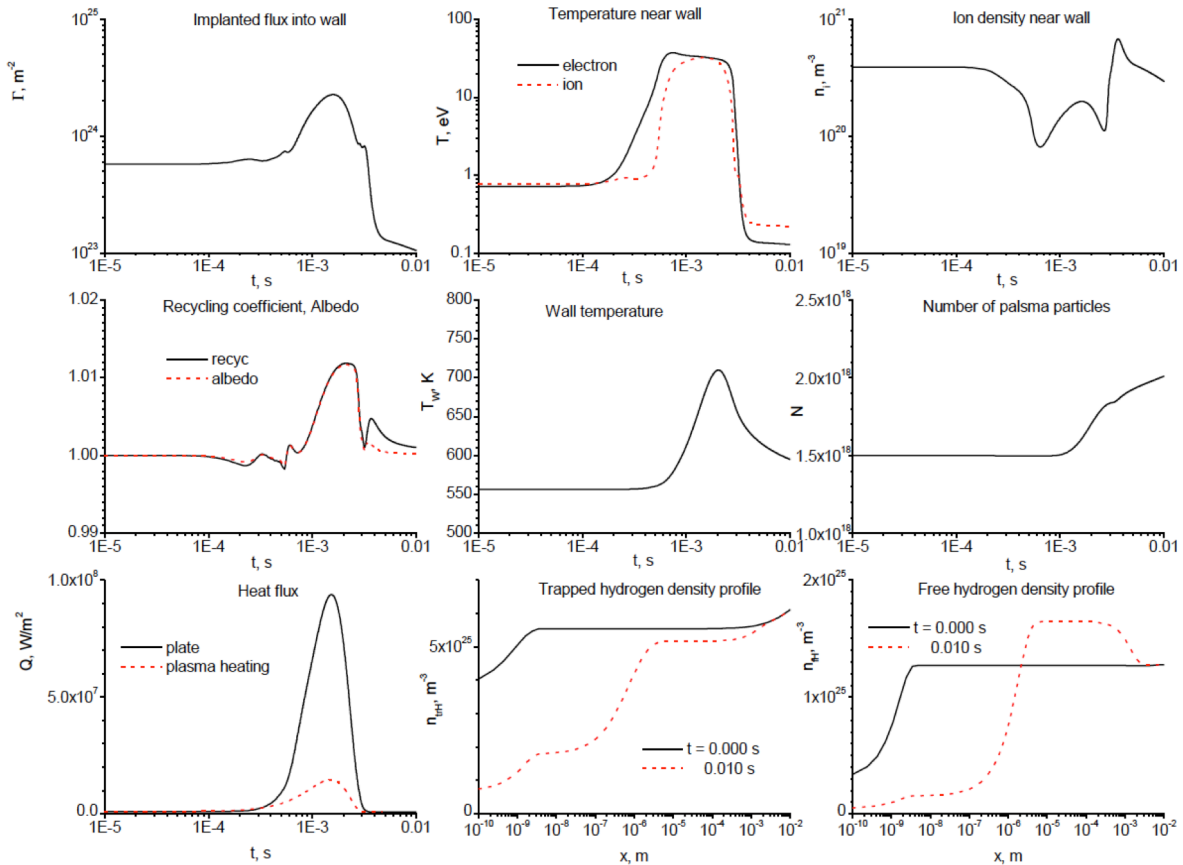


Figure 13. Time variation of plasma parameters and hydrogen profiles in tungsten wall for an ELM-like heat pulse with 1.5×10^{18} plasma particles.

Development of COGENT ELM model: We have implemented an ELM heat pulse model within the guiding center COGENT code. The model uses kinetic guiding center ions, and it can either use a Boltzmann electron model or kinetic guiding center electrons. We are verifying the model by reproducing the well-known ELM benchmark problem of simulating an ELM heat pulse for conditions relevant to the JET tokamak pedestal and SOL first initiated in Ref. [16]. The COGENT prediction for the heat flux using the 1D+2V kinetic ion and Boltzmann electron model is shown in Figure 14. We have shown that our 1D+2V results quantitatively agree with a number of previous studies at the 10% level, which is expected given variation in assumptions and in the numerical methods. Our work on this benchmark case has resulted in a publication [17] and a solicited talk at the 2018 American Physical Society Division of Plasma Physics Miniconference on Plasma-Materials Interactions in Fusion Devices: ITER and Beyond.

We have extended the COGENT ELM simulations to include both gyrokinetic ions and gyrokinetic electrons. These simulations are challenging due to short temporal and spatial scales associated with the electron dynamics, which introduces plasma waves and Alfvén waves into the system. The plasma waves are eliminated by using the gyro-Poisson equation instead of the full Poisson equation, while the Debye length scales are eliminated by using sheath boundary conditions that only allow electrons to reach the material surface if they have enough kinetic energy to exceed the electrostatic barrier at the sheath.

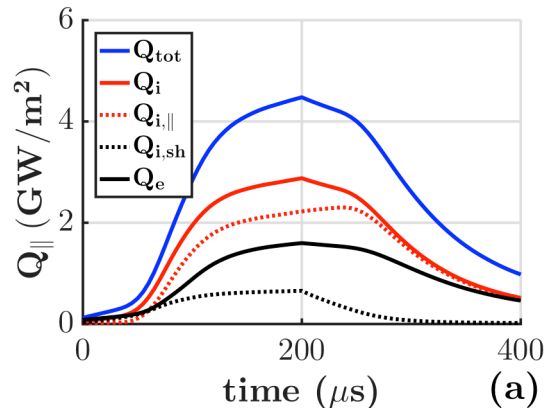


Figure 14. Cogent predictions of the heat flux generated by a 0.4 MJ ELM for a benchmark case for the JET tokamak. Collisionless simulation results with kinetics ions and Boltzmann electrons are shown for the total heat flux (blue), the total ion heat flux (solid red), the ion heat flux incident on the sheath (dotted red), the additional ion sheath heat flux (dotted black), and the electron heat flux (solid black).

behavior, and extend the activities currently underway with increased coordination between the Task 2 and Task 3 researchers. Development of the divertor-relevant BOUT++ turbulence model and the ELM-relevant heat pulse model within COGENT will be completed by the end of FY19. The BOUT++ turbulence physics model includes drift-resistive ballooning physics and linear sheath boundary conditions that drive preseath turbulence modes such as the conducting wall mode. A neutral fluid physics module has been added and the impact of neutrals on linear growth rates and nonlinear turbulence simulations will be performed over the remainder of the year. ELM heat pulse simulations have been performed using COGENT with kinetic ions, both Boltzmann electrons and kinetic electrons, and sheath boundary conditions. Over the remainder of the year we will complete our ELM heat pulse model and simulations with two kinetic species.

Discussion of Status of Year 2 & 3 milestones:

We now discuss the status of the year 2 & 3 milestones, which were documented in the proposal. Five main milestones/activities were proposed for the initial year of research activities. Table 1 provides a list of those milestones, along with a description of the status of the milestones.

Plans for Year 3 activities:

Overall, the project has had a very successful second year, as noted in the Executive summary, the project was both very productive and impactful on ITER and international fusion research efforts. During the coming year, we expect to continue to make progress at the atomic scale on discovering the behavior of helium and hydrogen below mixed material surfaces as a result of beryllium implantation, and to continue to refine the code coupling strategy for simulating plasma surface interactions, including the dynamic feedback of the surface to the edge plasma. In the next year, we will also perform a systematic uncertainty quantification of the coupled plasma surface interaction simulations of the ITER divertor, and extend our coupled PSI modeling to the WEST tokamak for experimental validation.

However, the equations still support extremely high frequency electrostatic Alfvén waves. These waves cause an unduly restrictive CFL condition for the time step (on the order of ns). The solution that we are presently exploring is to use a heuristic gyro-Poisson equation [18]. The more physically correct approach that we plan to implement is to obtain the correct electromagnetic Alfvén wave dispersion relation by adding the inductive parallel electric field ($-dA_{\parallel}/dt$) determined through Ohm’s law. The third route we are exploring is to treat the electron dynamics implicitly. An extension to COGENT’s ImEx capabilities to include both the parallel advection operator and the dynamics of the electric field is under development for the PSI2 SciDAC project, as described earlier in the CS/AM discussion.

Year 3 focus: Ongoing and future activities within Task 3 will continue to focus on the dynamic coupling of edge plasma and surface

Table 1. Summary of the proposed year 2 milestones, along with a description of the status and plans for successful completion.

Milestone descriptions	Status
UQ assessment of H-He-defect reaction rate constants on He bubble population and H inventory	As indicated earlier in the results for Task 1, UQ assessment of the influence of helium cluster diffusivity on total helium retention have been initiated, and will be expanded in the coming year to complete this milestone activity.
Initial parameterization of W-Be-H-He IAP, targeted MD/AMD simulations of H diffusion and trapping behavior; KMC/MD models of PFC thermal-mechanical properties for representative sub-surface gas bubble and defect populations	As documented earlier in the report, the initial SNAP Be-W potential has been implemented to evaluate the impact of beryllium implantation on tungsten surfaces. Likewise, good progress has been made on developing the atomistic framework for evaluating the effect of helium bubble populations on tungsten elastic properties. Work is in progress to parameterize a W-H and W-Be-H SNAP interatomic potential, and the task 1 activities continue to make good progress in identifying atomistic mechanisms of helium bubble evolution and hydrogen interactions. These results will provide additional benchmarking data for the Xolotl code.
Coupled boundary plasma-surface evolution simulations with impurity transport modeling of DIII-D tungsten divertor ring experiments	As noted in Figure 10 and 11, initial efforts to model the tungsten source and transport in the metal ring campaign of DIII-D have been performed, with activities planned in the future to fully utilize SciDAC PSI codes.
Initial extension of coupled PMI simulations to mixed materials; implement and test coupling strategies for studies of materials erosion under transient conditions relevant to ELMs; initial physics studies of surface evolution under transient plasma conditions	As noted previously in the report, we are making progress in performing atomistic studies of Be-W mixed materials (Fig. 5) which will inform Xolotl simulations, and we are on track to begin evaluating mixed materials PSI. We also are underway in evaluating ELM conditions and testing the appropriate coupling strategies for dynamic conditions of PSIs involving transient conditions.
Implement non-linear, multi-species collision operator in hPIC; implement and test coupling strategies for dynamic BOUT++ plasma-wall models in simple geometries to compare with dynamic H outgassing measurements on PISCES	Development of the divertor-relevant BOUT++ turbulence model and the ELM-relevant heat pulse model within COGENT will be completed by the end of FY19. The BOUT++ turbulence physics model includes drift-resistive ballooning physics and linear sheath boundary conditions that drive pre-sheath turbulence modes such as the conducting wall mode. A neutral fluid physics module has been added and the impact of neutrals on linear growth rates and nonlinear turbulence simulations will be performed over the remainder of the year. ELM heat pulse simulations have been performed using COGENT with kinetic ions, both Boltzmann electrons and kinetic electrons, and sheath boundary conditions. Over the remainder of the year we will complete our ELM heat pulse model and simulations with two kinetic species.

REFERENCES CITED

- [1] <https://science.osti.gov/fes/community-resources/>
- [2] M. J. Baldwin, R. P. Doerner, D. Nishijima, D. Buchenauer, W. M. Clift, R. A. Causey, and K. Schmid, *J. Nucl. Mater.* 363-365, 1179 (2007).
- [3] M. A. Wood, M. A. Cusentino, B. D. Wirth, and A. P. Thompson, “Data-driven material models for atomistic simulation”, *Phys. Rev. B.* 99, 184305 (2019).
- [4] J. F. Ziegler, J. P. Biersack, and U. Littmark, “The Stopping and Range of Ions in Solids”, Springer, Morrisville (2008).
- [5] Li-Fang Wang et al., “Embedded-Atom Method Potential for Modeling Hydrogen and Hydrogen-Defect Interaction in Tungsten.” *Journal of Physics: Condensed Matter* 29, 43 (2017): 435401.
- [6] N. Juslin. “Analytical Interatomic Potential for Modeling Nonequilibrium Processes in the W-C-H System.” *Journal of Applied Physics* 98(12) (2005): 123520.
- [7] J. Guterl et al. “Modeling of Hydrogen Desorption from Tungsten Surface.” *Journal of Nuclear Materials* 463 (2015): 263–267.
- [8] K. D. Hammond, S. Blondel, L. Hu, D. Maroudas, and B. D. Wirth, “Large-scale atomistic simulations of low-energy helium implantation into tungsten single crystals,” *Acta Materialia* **144**, 561-578 (2018).
- [9] G. Henkelman, B.P. Uberuaga, and H. Jónsson, *J. Chem. Phys.* **113**, 9901 (2000).
- [10] D. Terentyev, V. Dubinko, A. Bakaev, Y. Zayachuk, W. Van Renterghem, and P. Grigorev, *Nucl. Fusion* **54**, (2014).
- [11] J. Guterl, T. Abrams, et al., *ERO modeling and analysis of tungsten erosion and migration from a toroidally symmetric source in DIII-D divertor*, Nuclear Fusion, submitted (2019)
- [12] G.L. Xu, J. Guterl, et al., *Modeling of inter- and intra-ELM tungsten erosion during DIII-D H-mode discharges* Nuclear Fusion, submitted (2019)
- [13] J. Guterl, P. Snyder, *On the prompt redeposition of tungsten in tokamak divertor*, PPCF, in preparation (2019)
- [14] J. Guterl, et al., *Reduced model of high-Z impurity redeposition and erosion in tokamak divertor and its application to DIII-D experiments*, PPCF, submitted (2019)
- [15] D. A. Russell, D. A. D’Ippolito, J. R. Myra, et al., *Phys. Plasmas* **22**, 092311 (2015).
- [16] R. A. Pitts, J. P. Coad, D. P. Coster, et al., *Plasma Phys. Control. Fusion* **47**, B303 (2005).
- [17] I. Joseph, M. A. Dorf, M. R. Dorr, “Simulation of edge localized mode heat pulse using drift-kinetic ions and Boltzmann electrons,” *Nucl. Mater. Energy* **19**, 300 (2019).
- [18] E. L. Shi, A. H. Hakim, and G. W. Hammett, *Phys. Plasmas* **22**, 022504 (2015).

Appendix 1: Project Bibliography

Peer-Reviewed, Archival Journal Publications:

- K. D. Hammond, I. V. Naeger, W. Widanagamaachchi, L.-T. Lo, D. Maroudas, and B. D. Wirth, [Flux Effects on Helium Bubble Growth and Surface Morphology in Plasma-Facing Tungsten from Large-Scale Molecular Dynamics Simulations](#), *Nuclear Fusion* **59** (6): 066035 (2019).
- D. Maroudas and B. D. Wirth, “Atomic-Scale Modeling toward Enabling Models of Surface Nanostructure Formation in Plasma-Facing Materials,” *Current Opinion in Chemical Engineering* **23**, 77-84 (2019).
- M.A. Wood, M.A. Cusentino, B.D. Wirth, and A. Thompson, “[Data-driven material models for atomistic simulations](#)”, *Physical Review B* **99** (2019) 184305
- Z. J. Bergstrom, C. Li, G. D. Samolyuk, B. P. Uberuaga, and B. D. Wirth, [Hydrogen interactions with low-index surface orientations of tungsten](#), *Journal of Physics: Condensed Matter* **31** (25): 255002 (2019).
- I. Joseph, M. A. Dorf, and M. R. Dorr, [Simulation of Edge Localized Mode Heat Pulse Using Drift-Kinetic Ions and Boltzmann Electrons](#), *Nuclear Materials and Energy* **19**: 330–334 (2019).
- L. Yang, Z. J. Bergstrom, and B. D. Wirth, [Effect of Interatomic Potential on the Energetics of Hydrogen and Helium-Vacancy Complexes in Bulk, or Near Surfaces of Tungsten](#), *Journal of Nuclear Materials* **512**: 357–370 (2018).
- S. Blondel, D. E. Bernholdt, K. D. Hammond, and B. D. Wirth, [Continuum-Scale Modeling of Helium Bubble Bursting Under Plasma-Exposed Tungsten Surfaces](#), *Nuclear Fusion* **58** (12): 126034 (2018). [[corrigendum](#)]
- Z. Yang and K. D. Hammond, [Helium In-Plane Migration Behavior on {100} Symmetric Tilt Grain Boundaries in Tungsten](#), *Journal of Physics: Condensed Matter*, **30** (32): 325002 (2018).
- Z. Yang, L. Hu, D. Maroudas, and K. D. Hammond, [Helium Segregation and Transport Behavior Near Symmetric Tilt Grain Boundaries in Tungsten](#), *Journal of Applied Physics*, **123** (22): 225104 (2018).
- L. Yang and B. D. Wirth, [Energetics of Hydrogen and Helium-Vacancy Complexes in Bulk and Near Surfaces of Tungsten: First-Principles Study](#), *Journal of Applied Physics* **123** (21): 215104 (2018). (Featured Article)
- L. Yang, Z. J. Bergstrom, and B. D. Wirth, [First-Principles Study of Helium-Vacancy Complexes Below Tungsten Surfaces](#), *Journal of Applied Physics* **123** (20): 205108 (2018).
- S. I. Krasheninnikov, [On Numerical Study of Coupled Plasma-Wall Instability](#), *Physics of Plasmas* **25** (6): 064501 (2018). (Editor's Pick)
- J. Drobny, D. Curreli, [F-TRIDYN Simulations of Tungsten Self-Sputtering and Applications to Coupling Plasma and Material Codes](#), *Computational Materials Science*, **149** (15): 301–306 (2018).
- R. D. Smirnov and S. I. Krasheninnikov, [Stress-induced hydrogen self-trapping in tungsten](#), *Nuclear Fusion* **58** (12): 126016 (2018).
- O. Cekmer, K. Sargsyan, S. Blondel, H. Najm, D. Bernholdt, and B.D. Wirth, [Uncertainty quantification for incident helium flux in plasma-exposed tungsten](#), *International Journal for Uncertainty Quantification*, **8** (5): 429–446 (2018).
- Smith, C.W., Granzow, B., Diamond, G., Ibanez, D., Sahni, O., Jansen, K.E. and Shephard, M.S., 2018. [In-memory integration of existing software components for parallel adaptive unstructured mesh workflows](#). *Concurrency and Computation: Practice and Experience*, 30(18), p.e4510.
- Diamond, G., Smith, C.W., Yoon, E. and Shephard, M.S., 2018, November. [Dynamic Load Balancing of Plasma and Flow Simulations](#). In 2018 IEEE/ACM 9th Workshop on Latest Advances in Scalable Algorithms for Large-Scale Systems (scalA) (pp. 73-80). IEEE.

Presentations:

- Weerasinghe, L. Hu, B. D. Wirth, and D. Maroudas, “Effects of Helium Ion Irradiation on Thermal Properties of Tungsten,” 17th International Conference on Plasma Facing Materials and Components for Fusion Applications, May 2019, Eindhoven, the Netherlands.

- A. Weerasinghe, L. Hu, K. D. Hammond, B. D. Wirth, and D. Maroudas, “Analysis of Helium Segregation on Surfaces of Tungsten at Different Levels of Helium Ion Irradiation,” 17th International Conference on Plasma Facing Materials and Components for Fusion Applications, May 2019, Eindhoven, the Netherlands.
- D. Dasgupta, R. D. Kolasinski, C.-S. Wong, D. Maroudas, and B. D. Wirth, “Modeling of ‘Fuzz’ Formation in Plasma-Facing Materials,” 17th International Conference on Plasma Facing Materials and Components for Fusion Applications, May 2019, Eindhoven, the Netherlands.
- R. D. Kolasinski, D. Dasgupta, C.-S. Wong, R. Friddle, A. Engel, J. A. Whaley, D. A. Buchenauer, D. Maroudas, and B. D. Wirth, “Effects of Low-Fluence Helium Plasma Exposure Characterized by Helium Ion Microscopy, Scanning Probes, and Ellipsometry,” 17th International Conference on Plasma Facing Materials and Components for Fusion Applications, May 2019, Eindhoven, the Netherlands.
- M. V. Umansky and J. R. Myra, “Implementation and testing of SOLT3D model for tokamak edge turbulence,” 24th Joint US-EU Transport Task Force Meeting, Austin Texas, March 18-21, 2019.
- M.S. Shephard, et al., “Unstructured Mesh Support for Particle-in-Cell Simulations”, SIAM Computational Science and Engineering, Spokane, WA, February 26, 2019.
- Giridhar Nandipati, Wahyu Setyawan, Kenneth J Roche, Richard J Kurtz, Brian Wirth, [Effect of Trapping/Detrapping of SIA Clusters by Impurities on Damage Accumulation in Neutron Irradiated Tungsten: Comparison of 14 MeV-Neutron and High-Flux Isotope Reactor \(HFIR\) PKA Spectra](#), American Physical Society Division of Plasma Physics Annual Meeting, Portland, Oregon, November 7, 2018.
- Brandon Laufer, Karl D Hammond, [Simulation of the Effect of Hydrogen Repulsion on Clustering and Retention in Tungsten](#), American Physical Society Division of Plasma Physics Annual Meeting, Portland, Oregon, November 7, 2018.
- Roman Smirnov, Sergei Krasheninnikov, [Stress induced hydrogen self-trapping in tungsten](#), American Physical Society Division of Plasma Physics Annual Meeting, Portland, Oregon, November 7, 2018.
- Jerome Guterl, Sergei Krasheninnikov, Igor Bykov, Stefan A Bringuier, Philip B Snyder, [Theoretical study of hydrogen desorption from tungsten in divertor conditions](#), American Physical Society Division of Plasma Physics Annual Meeting, Portland, Oregon, November 7, 2018.
- David Martin, Mary Alice Cusentino, Brian Wirth, [Evaluating the Impact of Helium Bubble Layers on Hydrogen Diffusion](#), American Physical Society Division of Plasma Physics Annual Meeting, Portland, Oregon, November 7, 2018.
- Zachary Bergstrom, Li Yang, Brian Wirth, [H Binding Energetics at Near-Surface He-V clusters and Bubbles in Tungsten](#), American Physical Society Division of Plasma Physics Annual Meeting, Portland, Oregon, November 7, 2018.
- Sophie Blondel, David E Bernholdt, John Canik, Mark R Cianciosa, Davide Curreli, Jon T Drobny, Wael Elwasif, David L Green, Ane Laso, Philip C Roth, Tim Younkin, Brian Wirth, [Prediction of Near Surface Gas Bubble Evolution in the ITER Divertor with Cluster Dynamics](#), American Physical Society Division of Plasma Physics Annual Meeting, Portland, Oregon, November 7, 2018.
- Mitchell Wood, Mary Alice Cusentino, Aidan P Thompson, [Scale-bridging from the Atoms Up: Employing Machine Learning to Improve the Accuracy and Scalability of Molecular Dynamics](#), American Physical Society Division of Plasma Physics Annual Meeting, Portland, Oregon, November 7, 2018.
- Dimitrios Maroudas, Dwaipayan Dasgupta, Robert D Kolasinski, Brian D Wirth, [Modeling of Surface Morphological Evolution of Plasma-Facing Tungsten](#), American Physical Society Division of Plasma Physics Annual Meeting, Portland, Oregon, November 7, 2018.
- Jon T Drobny, Davide Curreli, Ane Laso, Sophie Blondel, John Canik, David L Green, Philip C Roth, Tim Younkin, Brian Wirth, [Applied Statistical Model of Surface Morphology for Plasma-Material Interactions](#), American Physical Society Division of Plasma Physics Annual Meeting, Portland, Oregon, November 7, 2018.
- Tim Younkin, Khachik Sargsyan, Tiernan Casey, Habib Nasri Najm, Russ Doerner, Daisuke Nishijima, David L Green, John Canik, Ane Laso, Philip C Roth, Davide Curreli, Jon T Drobny, Parker Forehand,

- Brian Wirth, [Quantification on the Effect of Uncertainty On Impurity Migration In PISCES-A Simulated With GITR](#), American Physical Society Division of Plasma Physics Annual Meeting, Portland, Oregon, November 7, 2018.
- Blas Pedro Uberuaga, Xiang-Yang Liu, Luis Sandoval, Danny Perez, Arthur F. Voter, [Using Accelerated Molecular Dynamics Simulations to Understand Helium Bubble Evolution in Tungsten](#), American Physical Society Division of Plasma Physics Annual Meeting, Portland, Oregon, November 7, 2018.
 - Robert D Kolasinski, Dwaipayan Dasgupta, Josh A Whaley, Aaron Engel, Frances I Allen, Dean Alan Buchenauer, Dimitrios Maroudas, Brian Wirth, [Effects of helium plasmas on tungsten surfaces characterized by helium ion microscopy, ion channeling, and in-situ spectroscopic ellipsometry](#), American Physical Society Division of Plasma Physics Annual Meeting, Portland, Oregon, November 7, 2018.
 - Karl D Hammond, Ian V Naeger, Wathsala Widanagamaachchi, Li-Ta Lo, Dimitrios Maroudas, Brian D. Wirth, [Flux Effects on Helium-Induced Surface Evolution in Tungsten](#), American Physical Society Division of Plasma Physics Annual Meeting, Portland, Oregon, November 7, 2018.
 - Russell Doerner, Sergei Krasheninnikov, Matthew Baldwin, Daisuke Nishijima, Marlene Patino, [Using ³He-containing plasma to track the motion of helium atoms in tungsten](#), American Physical Society Division of Plasma Physics Annual Meeting, Portland, Oregon, November 7, 2018.
 - Andrei I Smolyakov, Sergei Krasheninnikov, [SOL ballooning instabilities due to sheath boundary conditions and X-point geometry](#), American Physical Society Division of Plasma Physics Annual Meeting, Portland, Oregon, November 6, 2018.
 - Ilon Joseph, Mikhail Dorf, Milo Dorr, [Kinetic heat pulse propagation in the tokamak scrape-off layer](#), American Physical Society Division of Plasma Physics Annual Meeting, Portland, Oregon, November 6, 2018.
 - Sergei Krasheninnikov, [On coupled plasma-wall instabilities](#), American Physical Society Division of Plasma Physics Annual Meeting, Portland, Oregon, November 6, 2018.
 - Brian Wirth, [Multiscale Modeling of Plasma Surface Interactions with Coupled Boundary Plasma Physics](#), American Physical Society Division of Plasma Physics Annual Meeting, Portland, Oregon, November 6, 2018.
 - Davide Curreli, Jon T Drobny, Ane Lasa, Sophie Blondel, John Canik, David L Green, Tim Younkin, Brian Wirth, [Coupled PIC-BCA simulations of the near-surface plasma at the ITER Outer Target](#), American Physical Society Division of Plasma Physics Annual Meeting, Portland, Oregon, November 6, 2018.
 - John Canik, Ane Lasa, Sophie Blondel, Mark R Cianciosa, Davide Curreli, Jon T Drobny, Wael Elwasif, David L Green, Philip C Roth, Tim Younkin, Brian Wirth, Russ Doerner, Daisuke Nishijima, Matthew Baldwin, [Status of integrated simulation of PFC surface evolution within the PSI-SciDAC project](#), American Physical Society Division of Plasma Physics Annual Meeting, Portland, Oregon, November 6, 2018.
 - M.S. Shephard, E. Yoon, E.S. Seol, A. Truszkowska, G. Perumpilly, O. Sahni, W. Tobin, [Distributed Mesh Infrastructure for Particle-in-Cell Simulations](#), APS DPP meeting, Portland, OR, Nov. 6, 2018.
 - L. Hu, A. Weerasinghe, K. D. Hammond, B. D. Wirth, and D. Maroudas, “Analysis of Helium Segregation on Surfaces of Plasma-Exposed Tungsten,” AICHE Annual Meeting, October-November 2018, Pittsburgh, Pennsylvania.
 - D. Dasgupta, R. D. Kolasinski, D. Maroudas, and B. D. Wirth, “Modeling of Surface Morphological Evolution of Plasma-Facing Tungsten in Fusion Reactors,” AICHE Annual Meeting, October-November 2018, Pittsburgh, Pennsylvania.
 - K. D. Hammond, I. V. Naeger, D. Ruff, S. Blondel, D. Maroudas, and B. D. Wirth, “Effects of Flux on Helium Bubble Growth in Plasma-Facing Materials,” AICHE Annual Meeting, October-November 2018, Pittsburgh, Pennsylvania.
 - [PSI SciDAC: Predicting the Performance and Impact of Dynamic PFC Surfaces](#)- Brian Wirth, SciDAC PI Meeting 2018, Rockville, Maryland.

- [PSI2 SciDAC — Integrating Codes to Model Plasma Surface Interactions: focus on Plasma Sheath Effects and Sputtering Near Surfaces](#) - Davide Curreli, SciDAC PI Meeting 2018, Rockville, Maryland. [\(LowRes\)](#) [\(HighRes\)](#)
- [Plasma Surface Interactions SciDAC: Dynamic plasma material surface interactions at the edge of a magnetically confined fusion reactor](#) - Ilon Joseph, SciDAC PI Meeting 2018, Rockville, Maryland.
- M.S. Shephard, et. al., Unstructured Mesh Technologies for Fusion Simulation Codes, SciDAC PI Meeting, Washington, DC, July 24, 2018.
- M.S. Shephard, et al., Distributed Mesh Infrastructure for Particle-in-Cell Simulations, SIAM Annual Meeting, Portland, OR, July 9, 2018.
- D. Dasgupta, R. D. Kolasinski, D. Maroudas, and B. D. Wirth, “Modeling of Fuzz Formation in Helium-Ion-Irradiated Tungsten,” 23rd International Conference on Plasma-Surface Interactions in Controlled Fusion Devices (PSI-23), June 2018, Princeton, New Jersey.